Research Square

Preprints are preliminary reports that have not undergone peer review.
They should not be considered conclusive, used to inform clinical practice,
or referenced by the media as validated information.

Exploring Ferroptotic Vulnerabilities in Pediatric Cancer Through Clinical Biochemistry Using the Roche cobas® 8000

Cristina Banella

cristina.banella@meyer.it

Meyer Children's Hospital IRCCS

Maria Ascone

Meyer Children's Hospital IRCCS

Lorenzo Barbetti

Meyer Children's Hospital IRCCS

Amada Pasha

Meyer Children's Hospital IRCCS

Grazia Riccardi

Meyer Children's Hospital IRCCS

Francesco Pegoraro

Meyer Children's Hospital IRCCS

Luca Mannelli

Meyer Children's Hospital IRCCS

Rachele Amato

Meyer Children's Hospital IRCCS

Perla Scalini

Meyer Children's Hospital IRCCS

Serena Travaglini

University of Rome Tor Vergata

Brunella Pagliazzi

Meyer Children's Hospital IRCCS

Laura Becciolini

Meyer Children's Hospital IRCCS

Marinella Veltroni

Meyer Children's Hospital IRCCS

Annalisa Tondo

Meyer Children's Hospital IRCCS

Franco Bambi

Meyer Children’s Hospital IRCCS

Maura Calvani

Meyer Children’s Hospital IRCCS

Method Article

Keywords: Ferroptosis, Cancer, Metabolism, Iron, Cobas800, Ferritin, Translational Medicine

Posted Date: November 25th, 2026

DOI: https://doi.org/10.21203/rs.3.rs-11528068/v1

License: This work is licensed under a Creative Commons Attribution 4.0 International License.
Read Full License

Additional Declarations: No competing interests reported.

Exploring Ferroptotic Vulnerabilities in Pediatric Cancer Through Clinical Biochemistry Using the Roche cobas® 8000

Cristina Banella[1†*], Maria Ascone[1†], Lorenzo Barbetti[2], Amada Pasha[1,3], Grazia Riccardi[2], Francesco Pegoraro[1], Luca Mannelli[2], Rachele Amato[1], Perla Scalini[1], Serena Travaglini[4], Brunella Pagliazzi[2], Laura Becciolini[2], Marinella Veltroni[1], Annalisa Tondo[1], Franco Bambi[2,5#], Maura Calvani[1#].

[1]Department of Pediatric Hematology-Oncology, Meyer Children's Hospital IRCCS, 50139, Florence, Italy.

[2] Clinical Chemistry and Microbiology Laboratory, Meyer Children's Hospital IRCCS, 50139, Florence, Italy.

[3] Department of Experimental and Clinical Biomedical Sciences, University of Florence, 50139, Florence, Italy.

[4]Department of Experimental Medicine, University of Rome Tor Vergata, 00133, Rome, Italy

[5]Transfusion Medicine and Laboratory Unit, Meyer Children's Hospital IRCCS, 50139, Florence, Italy.

[†] C.B. and M.A. contributed equally to this work.

[#] F.B. and M.C. are co-last authors.

[*] Corresponding author: cristina.banella@meyer.it (C.B.); Department of Pediatric Hematology-Oncology, Meyer Children's Hospital IRCCS, 50139, Florence, Italy.

Abstract

Background Ferroptosis is an iron-dependent-regulated cell death increasingly recognized as a potential therapeutic vulnerability in pediatric cancer. However, the clinical translation of ferroptosis research remains limited because canonical ferroptosis markers, such as GPX4 depletion and lipid peroxidation, are not routinely measurable in standard diagnostic laboratories. In contrast, alterations in iron metabolism and metabolic reprogramming associated with ferroptosis susceptibility may be assessed through clinically accessible biomarkers.

Methods We evaluated the Roche Cobas® 8000 analyzer as a translational platform for the biochemical profiling of ferroptosis-associated metabolic states in pediatric cancer models. The system was used to quantify iron metabolism and metabolic biomarkers, including circulating iron species (Fe2+/Fe3+), ferritin (FTH1), transferrin (TRF1), lactate dehydrogenase A (LDHA), and

lactate, in treated and untreated samples. Analytical performance, sample processing efficiency, and multiparametric profiling capabilities were assessed within a standardized clinical workflow.

Results The Cobas® 8000 platform enabled rapid and reproducible quantification of multiple iron-related and metabolic parameters using minimal sample volumes. Distinct biochemical and metabolic alterations were identified between experimental conditions, revealing patterns consistent with ferroptosis-associated vulnerabilities. The automated and standardized nature of the platform reduced pre-analytical variability and supported robust comparative profiling across samples.

Conclusions Although the Roche Cobas® 8000 analyzer does not measure canonical ferroptosis markers, it provides clinically accessible metabolic and iron-related profiling that may identify biological states associated with ferroptosis susceptibility. This approach represents a practical bridge between experimental ferroptosis research and clinical oncology, supporting the translational development of ferroptosis-oriented therapeutic strategies in pediatric cancer.

Keywords: Ferroptosis, Cancer, Metabolism, Iron, Cobas800, Ferritin, Translational Medicine.

1. Introduction

Recent discoveries on iron's role in tumor processes and the emergence of ferroptosis as a cell death mechanism have revolutionized our understanding of cellular dynamics in cancer [1–7]. Iron acts as an essential element for several fundamental biological processes in living organisms. Its unique chemical properties enable oxygen transport and participation in essential biochemical reactions. Iron's importance extends far beyond simple oxygen transport, as it participates in multiple metabolic reactions, particularly those within mitochondria, the cellular energy center [8–11]. Research highlights the pleiotropic functions of iron, showing its fundamental role in protective immune responses against tumors as well as its involvement in dysregulated processes that promote cancer progression. This duality makes iron metabolism crucial for understanding cancer biology and developing new therapeutic strategies. Furthermore, iron plays a crucial role in a form of programmed cell death called “ferroptosis” [12,13].

In 2012, Dixon et al. described ferroptosis as an iron-dependent regulated cell death characterized by excessive lipid peroxidation [14]. Unlike other cell death mechanisms, ferroptotic cells exhibit distinctive morphological changes, including ruptured outer mitochondrial membranes, shrinkage, and reduced or absent mitochondrial cristae. At the cellular level, ferroptosis involves iron ion accumulation, high reactive oxygen species (ROS), decreased NADPH, and alterations in specific gene expression.

Cancer cells are particularly vulnerable to ferroptosis due to their elevated iron requirements, accelerated metabolism, and increased ROS production. Research indicates that ferroptosis induction can inhibit tumor growth and enhance chemosensitivity, making it a promising therapeutic approach. This characteristic represents an "Achilles' heel" for resistant tumor cells, making them susceptible to ferroptosis-inducing mechanisms. By sequestering excess iron, FTH1 not only ensures iron availability for essential metabolic functions but also protects macromolecules such as DNA, proteins, and lipids from iron-mediated oxidative damage [15]. Altered FTH1 levels are frequently observed in clinical settings, usually reflecting disruptions in iron regulation, and increasing evidence highlights its involvement in a broad spectrum of pathological conditions, ranging from inflammation to neurodegeneration and cancer [16–18].

The evaluation of iron metabolism and its regulatory components—including FTH1, transferrin (TRF1), and soluble transferrin receptor (sTfR)—relies on various methodologies with different applicability in translational research [19].

For intracellular iron measurement, researchers performed colorimetric assays such as ferrozine-based methods to detect Fe^{2+} by generating a colored complex. Although these assays provide a cost-effective approach for measuring total cellular iron content, they lack sufficient resolution to differentiate between specific subcellular iron pools or to assess iron distribution within cellular compartments [20]. While fluorescent probes like Calcein-AM effectively detect labile iron pools, they are subjected to several analytical limitations, including pH-dependent fluorescence variability and interference from endogenous cellular components that cause non-specific quenching artifacts [21]. Mass spectrometry techniques, particularly Inductively Coupled Plasma Mass Spectrometry (ICP-MS), provide quantitative data on total iron content with high sensitivity. Still, it requires extensive sample preparation, and it's unable to differentiate between free and protein-bound iron forms [22–25]. For FTH1, TRF1, and sTfR analysis, protein-level techniques include WB and immunofluorescence (IF) using specific antibodies, which provide isoform-specific data, but it remains semi-quantitative and labor-intensive work [26]. Functional genomic approaches include gene silencing methods such as siRNA or CRISPR-Cas9 to clarify the roles of iron regulators in cellular processes [27,28]. Next-generation sequencing (NGS) technologies assess transcriptional networks linking iron metabolism to ferroptosis. In contrast, long-read sequencing platforms like Oxford Nanopore Technologies can identify structural variants and methylation changes affecting iron-related genes [29,30].

Despite their utility in cell line models, these methodologies show significant challenges when applied to primary patient samples. Clinical specimens are often limited, yielding insufficient material for bulk analyses like ICP-MS or NGS. Time sensitivity is another critical factor, as delays in processing can alter iron distribution and FTH1 stability [31,32]. Moreover, tumor microenvironments are characterized by cellular heterogeneity, leading to mixed populations with varying iron metabolism patterns that conventional bulk analyses may fail to detect accurately [33–35].

In this setting, an accurate assessment of iron metabolism is critical in both research and clinical practice, particularly in oncology, inflammatory diseases, and anemia management. The Roche Cobas® 8000 analyzer, a diagnostic platform widely implemented in clinical laboratories worldwide, has emerged as a valuable tool for high-throughput evaluation of iron-related and metabolic biomarkers, including circulating iron species (Fe2+ and Fe3+), ferritin (FTH1), transferrin (TRF1), soluble transferrin receptor (sTfR), lactate dehydrogenase A (LDHA), and

lactate. Furthermore, the Cobas® 8000 platform is not intended to directly measure canonical ferroptosis markers such as GPX4 depletion, lipid peroxidation, or ferroptotic membrane damage. Instead, its measure the biochemical and metabolic consequences associated with ferroptosis susceptibility, particularly alterations in iron handling and metabolic reprogramming. From a translational perspective, this represents a major advantage rather than a limitation, as the clinically relevant challenge is not merely to demonstrate ferroptosis mechanistically, but to identify tumors and patients that may be biologically vulnerable to ferroptosis-inducing strategies. By requiring minimal sample volumes and enabling simultaneous quantification of multiple clinically standardized parameters, the Cobas® 8000 analyzer reduces pre-analytical variability and improves reproducibility across laboratories. Its rapid and automated processing of treated and untreated samples using the same specimen supports robust metabolic profiling in both experimental and clinical settings. This approach creates a practical bridge between bench research and bedside application, providing a scalable framework to investigate ferroptosis-associated vulnerabilities in pediatric oncology through clinically accessible biomarkers [36,37].

2. Establishing a method with a Cobas® 8000 for monitoring ferritin variation in cellular systems.

To achieve this objective, we first assessed whether the Roche Cobas® 8000 platform, which is primarily validated for serum and plasma samples, could reliably operate using non-conventional experimental matrices such as RIPA buffer supplemented with protease and phosphatase inhibitors. To exclude matrix-related analytical interference, the supplemented RIPA buffer was initially analyzed alone, showing no detectable ferritin signal. Subsequently, a ferritin sample with a known concentration (4910 ng/mL) was serially diluted in the same matrix to evaluate assay linearity and recovery. The measured concentrations showed a proportional decrease across dilutions, confirming the ability of the method to accurately discriminate ferritin levels within this experimental setting (Fig. 1a).

Following matrix validation, assay performance was further evaluated in biologically relevant samples using lysates obtained from the established human acute myeloid leukemia cell line MV4;11 (DSMZ, ACC 102), originally derived from a human leukemia specimen [38,39]. Detailed information on cell line provenance, molecular characteristics, and culture conditions is provided

in Supplementary Table S1 and the Supplementary Materials and Methods. Serial dilution of cellular lysates in supplemented RIPA buffer again demonstrated a proportional reduction in the measured signal across the tested dilution range, confirming that the Cobas® 8000 platform could reliably quantify ferritin also in complex cellular lysates (Fig. 1b). These findings support the applicability of the method not only in controlled analytical conditions, but also in experimental cellular systems relevant for translational oncology studies. Technically, the assay is based on a two-step sandwich phase. In the first incubation, 6 µL of the sample reacted with a biotinylated anti-ferritin monoclonal antibody and a ruthenium-labeled anti-ferritin monoclonal antibody, forming a ternary immune complex. In the second incubation, streptavidin-coated microparticles were added, allowing solid-phase capture through the high-affinity biotin–streptavidin interaction. The reaction mixture is then magnetically driven to the electrode surface, where unbound material was washed away with ProCell II M. Upon voltage application, the ruthenium complex triggers a chemiluminescent emission, which was quantified by a photomultiplier. Signal intensities were automatically converted into FTH1 concentrations using a two-point calibration curve and a master curve provided via Cobas® 8000 link (Fig. 1a). Performance validation showed an excellent analytical robustness (slope 0.9–1.1, intercept within ±2×LoB, correlation coefficient ≥0.95), as well as high sample stability (48 h at 20–25 °C, 7 days at 2–8 °C, and 12 months at –20 °C with up to two freeze–thaw cycles). Quality control was performed daily using PreciControl Tumor Marker or equivalent materials, according to laboratory requirements [40]. In addition, third-party independent controls InteliQ (multi-analyte human serum–based quality controls) were routinely employed, providing external validation beyond the manufacturer's internal standards. To ensure continuous analytical reliability, the system was subject to strict internal quality control procedures, routinely monitored through Levey–Jennings plots [41]. These charts displayed the daily performance of the FTH1 assay against predefined target values, allowing visualization of both short-term fluctuations and long-term trends. Each control run was evaluated based on the number of standard deviations from the mean (±1 SEM, ±2 SEM ±3 SEM), with Westgard rules applied to identify potential outliers. Typical oscillations within ±2 SEM were expected and reflected the biological variability of control materials, rather than analytical drift. In addition, the Cobas® 8000 software applies a moving target means to dynamically adapt control limits, thereby preventing false alarms while preserving sensitivity to real analytical shifts. Moreover, all operator interventions, including control replications, reagent cartridge calibrations, or replacements, were

automatically logged within the system, ensuring full traceability of the analytical process. These built-in safeguards further minimize operator-dependent bias and validate that the measurements reported here reflect true biological differences rather than technical artifacts (Fig. 1b). Importantly, no interference was observed from endogenous compounds, therapeutic iron levels (Fe^{2+}/Fe^{3+}), or commonly used drugs. Rare interferences due to heterophilic antibodies (anti-analyte, anti-streptavidin, or anti-ruthenium) have been reported in patient sera but were not detected in the context of cell lysates, highlighting the reliability of this adaptation (Table S1). As a proof of concept, we employed two established human cancer cell lines, A673 (Ewing sarcoma; ATCC, CRL-1598) and CCRF-CEM (T-cell acute lymphoblastic leukemia, T-ALL; ATCC, CCL-119), both originally derived from human tumor specimens.

To dissect the cellular response to ferroptotic stress, we performed two complementary experiments: a 24-h dose–response assay where cells were treated with increasing concentrations of erastin (0–40 μM), and a time-course experiment where a fixed dose of 10 μM was applied for intervals ranging from 0 to 240 min [42–44]. Cells were then pelleted, lysed in 250 μL of lysis buffer supplemented with a protease inhibitor cocktail, and centrifuged at 14,000 rpm for 30 min. The supernatants were then collected for analysis on the Cobas® 8000 platform. Notably, no further protein quantification was required, since the analyzer automatically calculates the analyte concentration in each sample (expressed in μg/L or ng/mL) against an internal calibration curve. The analytical range spans 0.50–2000 μg/L, defined by the lower limit of detection and the maximum of the master curve. Values below sensitivity were reported as <0.50 μg/L, while values exceeding the upper limit were indicated as >2000 μg/L—or, for diluted samples (1:50), up to 100,000 μg/L.

The assay required minimal sample volume (4–60 μL); however, to ensure reliable aspiration, at least 250 μL of lysate must be loaded into the dedicated vials. When smaller amounts are available, specific adapters can be employed to guarantee proper sampling. As shown in *Fig. 1 c-d*, FTH1 levels across a broad concentration/time range of erastin treatment were reliably quantified with excellent linearity over the tested interval, with both replicates demonstrating overlapping dose–response profiles. The assay discriminated accurately between low and high FTH1 concentrations, showing that the system can capture biologically relevant variations without loss of sensitivity. These data confirmed that the Cobas® 8000 methodology is suitable for precise quantification of

198 FTH1 in experimental samples, thereby providing a robust alternative to traditional antibody-based
199 techniques.

A

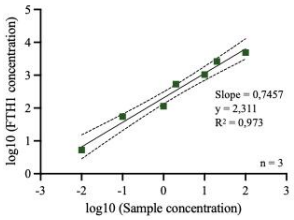
log10 (FTH1 concentration)
log10 (Sample concentration)
Slope = 0,7457
y = 2,311
R² = 0,973
n = 3

B

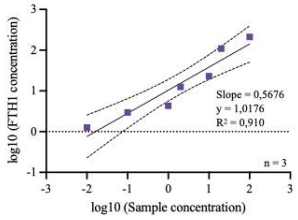
log10 (FTH1 concentration)
log10 (Sample concentration)
Slope = 0,5676
y = 1,0176
R² = 0,910
n = 3

C

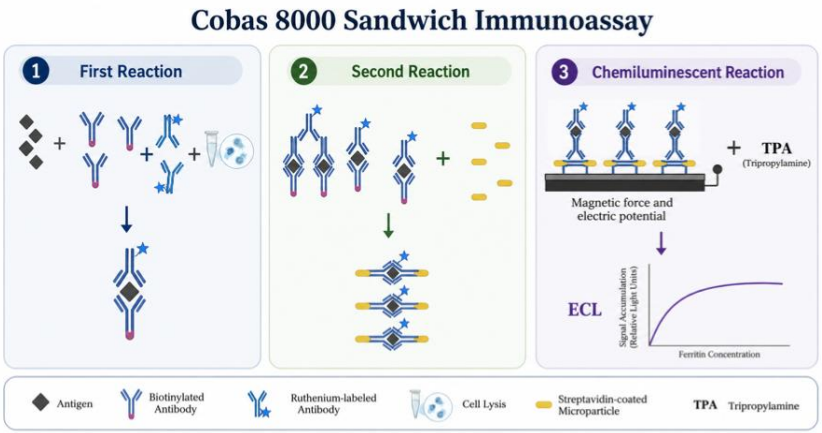
Cobas 8000 Sandwich Immunoassay
1 First Reaction
2 Second Reaction
3 Chemiluminescent Reaction
TPA
(Tripropylamine)
Magnetic force and
electric potential
ECL
Signal Accumulation
(Relative Light Units)
Ferritin Concentration
Antigen
Biotinylated
Antibody
Ruthenium-labeled
Antibody
Cell Lysis
Streptavidin-coated
Microparticle
TPA Tripropylamine

D

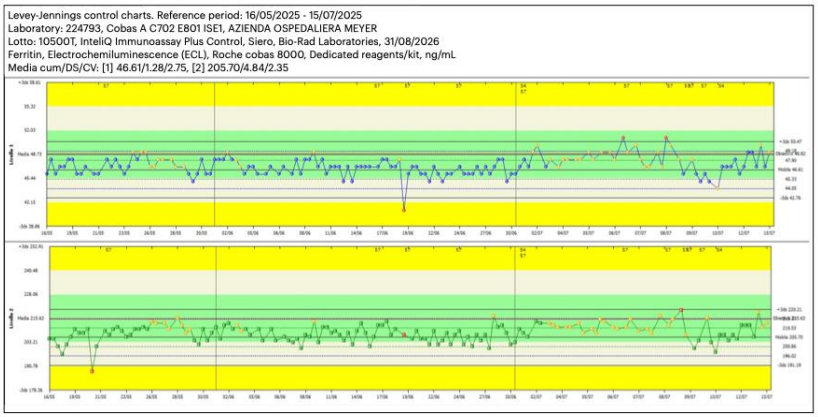
Levey-Jennings control charts. Reference period: 16/05/2025 - 15/07/2025
Laboratory: 224793, Cobas A C702 E801 ISE1, AZIENDA OSPEDALIERA MEYER
Lotto: 10500T, InteliQ Immunoassay Plus Control, Siero, Bio-Rad Laboratories, 31/08/2026
Ferritin, Electrochemiluminescence (ECL), Roche cobas 8000, Dedicated reagents/kit, ng/mL
Media cum/DS/CV: [1] 46.61/1.28/2.75, [2] 205.70/4.84/2.35

E

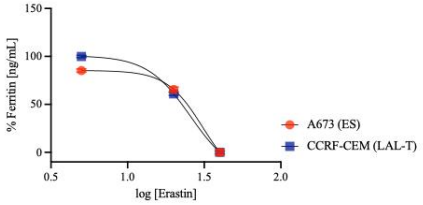
% Ferritin [ng/mL]
log [Erastin]
A673 (ES)
CCRF-CEM (LAL-T)

F

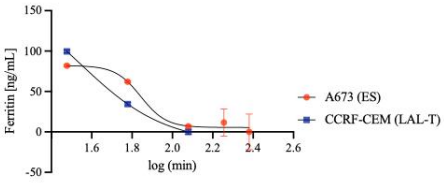
Ferritin [ng/mL]
log (min)
A673 (ES)
CCRF-CEM (LAL-T)

200

2.1. Development of Cobas® 8000 for free iron quantification in a cellular model

Another hallmark of ferroptosis is the release of free iron, which represents a key determinant of cellular susceptibility to this form of regulated cell death [45]. Free iron levels were quantified using the Cobas® 8000 platform through a colorimetric assay based on dual-wavelength measurement at 700/570 nm [46,47]. The analyte concentration was reported in µmol/L (also expressed as µg/dL or mg/L). Under acidic conditions (pH < 2), iron is dissociated from TRF1; in the presence of ascorbate, released Fe^{3+} ions are reduced to Fe^{2+}, which subsequently react with FerroZine to form a colored complex. The intensity of the chromogenic reaction is directly proportional to the iron concentration and can be measured photometrically (*Fig. 2a*). The assay covers a dynamic range of 0.90–179 µmol/L (5.00–1000 µg/dL, 0.05–10.0 mg/L). The lower detection limit corresponds to the minimum measurable concentration that can be distinguished from zero, defined as the lowest standard plus three standard deviations (standard 1 + 3 SEM repeatability, n = 21). In this setting, the sensitivity threshold was determined to be 0.90 µmol/L (5.00 µg/dL, 0.05 mg/L). However, certain interferences may affect the accuracy of iron measurement; these are detailed in *Table S2*.

As for FTH1, the analytical strength of the iron assay was ensured by constant internal monitoring, as illustrated by the Levey–Jennings control charts routinely generated through instrument calibration and quality control. These plots not only captured standard deviations and control targets but also logged operator interventions (e.g., control repetitions, cartridge recalibration, or replacement), ensuring full traceability and reproducibility of the measurements. A further technical advantage of this assay is its minimal sample requirement (4 µL in reduced mode, 8 µL in normal mode, and 17 µL in concentrated mode). When analyte concentrations exceeded the dynamic range, the system automatically performed dilution, reported the applied factor, and recalculated the final concentration. Moreover, unlike conventional iron assays that are highly photosensitive and require stringent protection from light exposure during handling, the Cobas® 8000 platform performs the reaction entirely within a closed and darkened chamber. This mechanism prevents photodegradation of the chromogenic complex and eliminates variability introduced by ambient light, thereby increasing the reliability of the assay.

To investigate ferroptosis-associated iron release, A673 and CCRF-CEM cells were exposed to the ferroptosis inducer erastin. Culture supernatants were harvested at defined time points, clarified by centrifugation at 1,200 rpm for 5 min to remove cells and debris, and subsequently analyzed on the

232 Cobas® 8000 platform. As shown in *Fig. 2B*, the assay was sensitive enough to capture temporal
233 fluctuations in extracellular iron following erastin treatment, demonstrating a progressive increase
234 in free iron release over time. These results confirm that Cobas-based detection is well suited to
235 monitor ferroptosis-associated iron dynamics with high sensitivity and reproducibility.

A

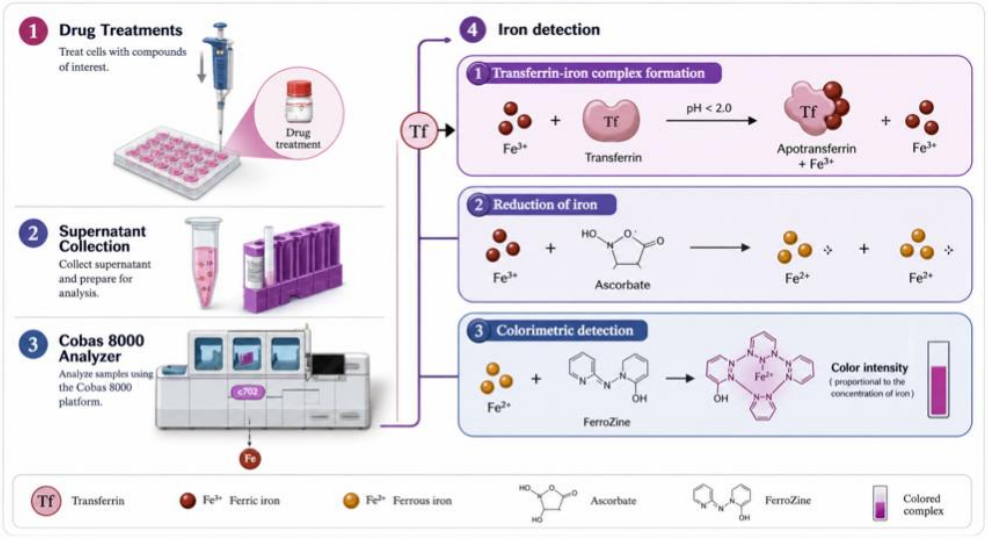

B

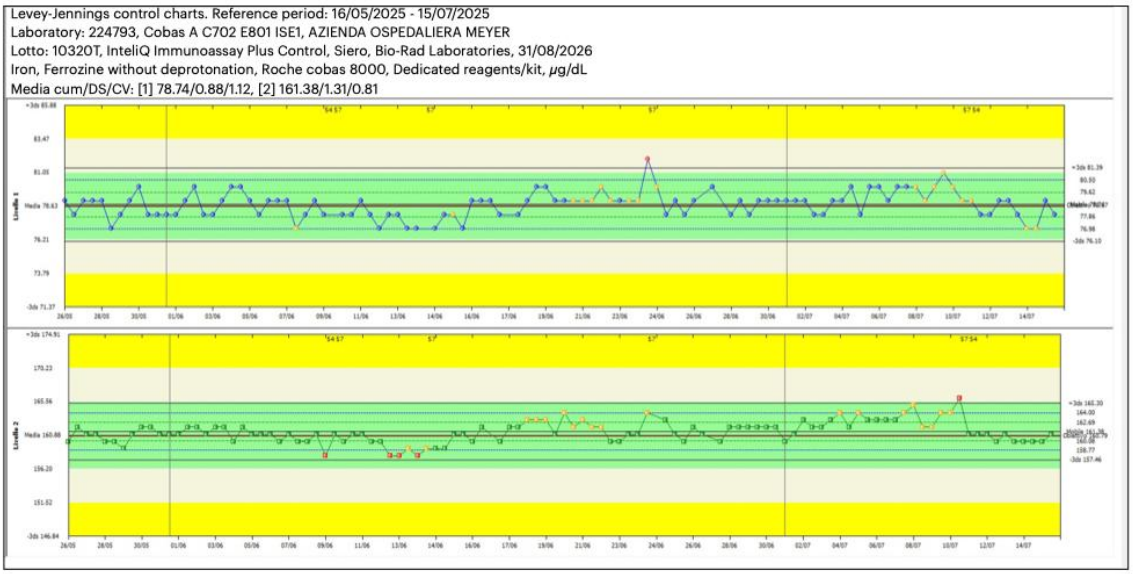

C

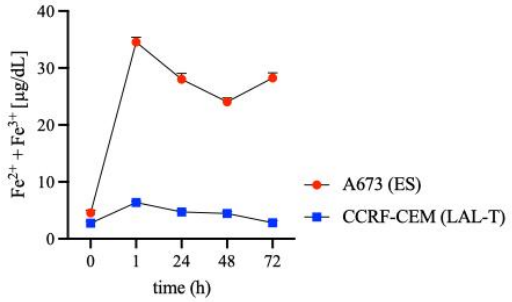

D

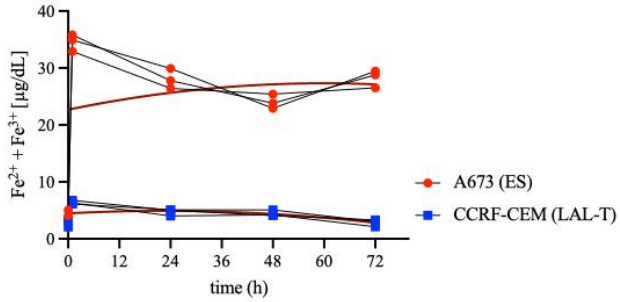

236

237 *2.2. Screening of Pediatric Cancer Cell Lines for Ferroptosis Sensitivity*

After confirming the analytical strength of the Cobas® 8000-based assay, we examined if pharmacological interventions could modulate ferroptotic pathways in pediatric cancer models. Specifically, we focused on the β3-adrenergic receptor (β3-AR) and its antagonist SR59230A (SR) for its antitumor properties and the evidence that β3-AR signaling sits at the crossroads of oxidative stress and lipid metabolism – two key drivers of ferroptosis. In our previous studies, our group has shown that β3-AR-blockade with SR has clear antitumor effects [48,49]. Importantly, Calvani et al. reported that selective inhibition of β3-AR led cancer cells to accumulate reactive ROS, triggering cell death [50]. Truly, β3-AR appears to play an "antioxidant" role in cells: its stimulation drives a glycolytic shift via mitochondrial uncoupling protein 2 (UCP2), whereas SR inhibits UCP2 and greatly raises mitochondrial ROS levels in cancer and stem cells [51]. Similarly, β3-AR is well known to regulate lipid handling – β3-AR activation in brown adipose tissue strongly promotes lipolysis and fatty acid oxidation [52,53]. Since ferroptosis is defined by iron-dependent lipid peroxidation and a redox imbalance, these observations suggested that β3-AR-blockade might induce a ferroptotic phenotype. In detail, SR raises ROS levels and perturbs fatty-acid metabolism; thus, we hypothesized that it could sensitize cancer cells to ferroptotic properties. Since β3-AR overexpression is associated with poor prognosis in pediatric malignancies, we hypothesized that SR might modulate ferroptosis-related processes.

Firstly, peripheral blood mononuclear cells (PBMCs) isolated from healthy donors were treated with SR 15 μM for 24 h. Supernatants were collected for free iron quantification, while cell pellets were lysed for FTH1 analysis. Neither intracellular FTH1 levels (*Fig. 3A*) nor extracellular iron release (*Fig. 3B*) showed significant differences compared to untreated controls. These results, supported by estimation plots, reinforce the absence of biologically meaningful effects in non-malignant cells. The use of estimation plots is particularly valuable in this context, as they provide effect-size visualization and confidence intervals, thereby complementing conventional p-values with a more informative representation of variability across biological replicates. Subsequently, we extended the analysis to a panel of pediatric cancer cell lines (*Table S3*) treated with SR 15 μM for 24 h.

A statistically significant reduction in FTH1 levels was observed in the FLT3-ITD^{+} acute myeloid leukemia (AML) cell line MV4;11 (*Fig. 3C*), in the T-cell acute lymphoblastic leukemia (T-ALL) models CCRF-CEM and MOLT-3 (ATCC, CRL-1552; *Fig. 3D*), in the Ewing sarcoma (ES) cell line A673 (*Fig. 3E*), and in the human neuroblastoma (NB) cell line BE(2)-C (ATCC, CRL-2268;

Fig. 3F). Both MOLT-3 and BE(2)-C are established human cancer cell lines originally derived from human tumor specimens. At the same time, no changes were detected in Jurkat cells (Fig. 3C). Conversely, free iron release increased in selected leukemia models and in ES. Still, it persisted unchanged in CCRF-CEM, Jurkat, and NB (*Fig. 3G-L*). Collectively, these data illustrate the ability of the Cobas® 8000 assay to discriminate between ferroptosis-sensitive and -resistant cellular contexts. SR treatment selectively triggered ferroptosis-associated signatures in subsets of pediatric cancer cells, while sparing healthy PBMCs. This highlights the potential of the platform for functional screening of ferroptosis-inducing compounds in relevant tumor models, paving the way for further mechanistic studies and orthogonal validation.

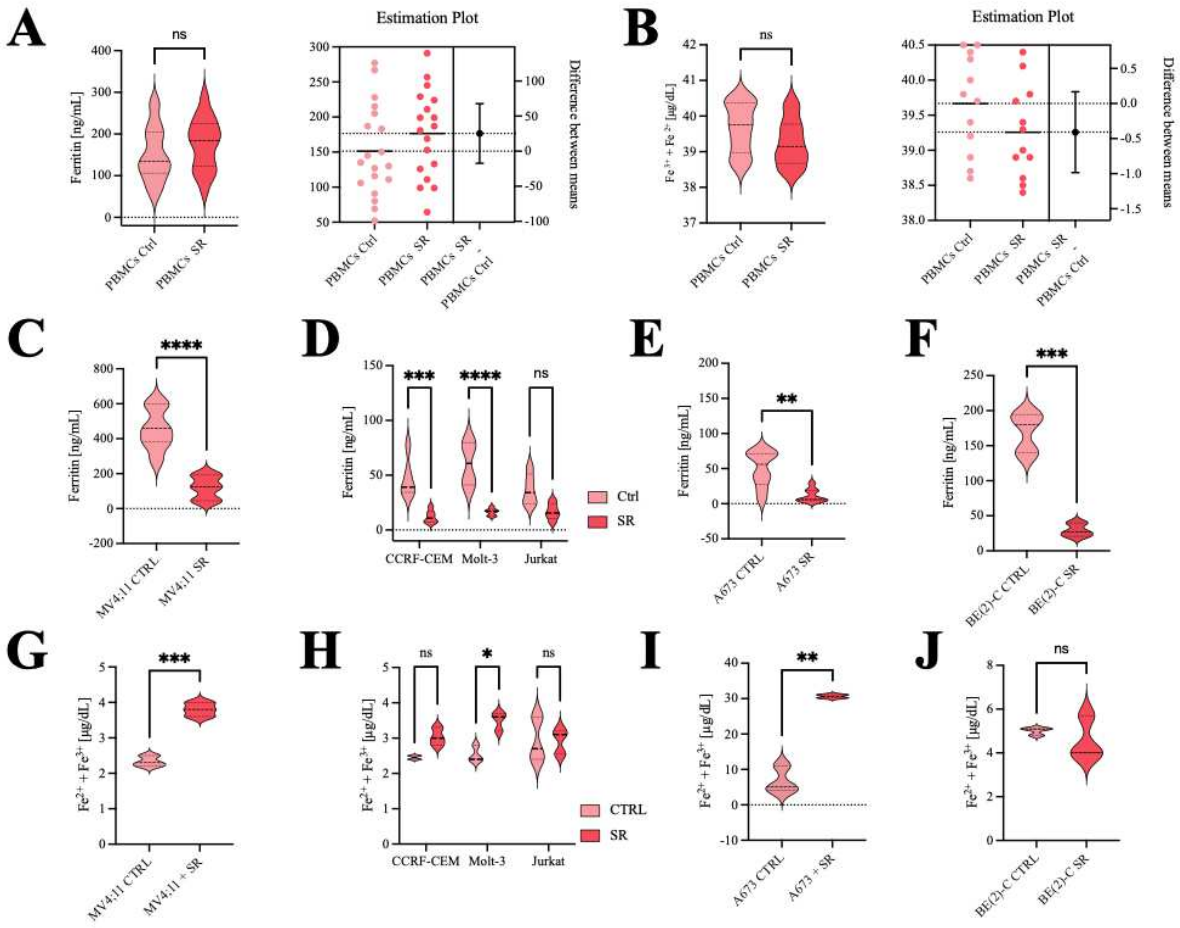

2.3. Cross-platform validation of ferritin measurements and ADRB3-dependent iron homeostasis

We validated Cobas® 8000-based ferritin measurements by immunoblotting for FTH1 in PBMC lysates (*Fig. 4A and Supplementary Figure S1 a,b*). FTH1 encodes the heavy subunit of ferritin, the major intracellular iron-storage protein, and its band intensity closely paralleled the Cobas®

8000 FTH1 values, confirming the absence of significant effects in non-malignant cells. Next, we compared basal FTH1 levels in wild-type (ADRB3+/+) versus ADRB3+/– BE(2)-C NB cells generated by CRISPR/Cas9-mediated gene editing. Under control conditions, ADRB3+/– cells exhibited significantly lower basal FTH1 than ADRB3+/+ cells (*Fig. 4B*). Treatment with the SR (10 or 15 μM) induced a dose-dependent rise in FTH1 in ADRB3+/+ cells but produced only a minimal increase in ADRB3+/– cells (*Fig. 4C*). Consistent with altered iron handling, iron release (Fe^{2+} + Fe^{3+}) into the culture medium increased with SR treatment in both genotypes but was higher in ADRB3+/+ cultures (*Fig. 4D*). WB analysis for FTH1 (*Fig. 4E and Supplementary Figure S1 c*) independently validated these findings: SR caused robust, dose-dependent FTH1 induction in ADRB3+/+ cells, whereas ADRB3+/– cells showed minimal response. Densitometric quantification (FTH1 normalized to β-actin) confirmed that ADRB3+/– cells had reduced baseline FTH1 and significantly blunted fold-induction compared to wild-type controls (*Fig. 4F–G*). Finally, RNA sequencing of ferroptosis-associated genes after SR treatment revealed cell-type-specific responses (*Fig. 4H–I*), with distinct regulatory patterns between ES and NB cells. These cross-platform validations demonstrate that ADRB3 deficiency lowers basal FTH1 and blunts iron homeostasis responses, supporting Cobas® 8000 measurements as a scalable tool for ferroptosis screening in cancer models.

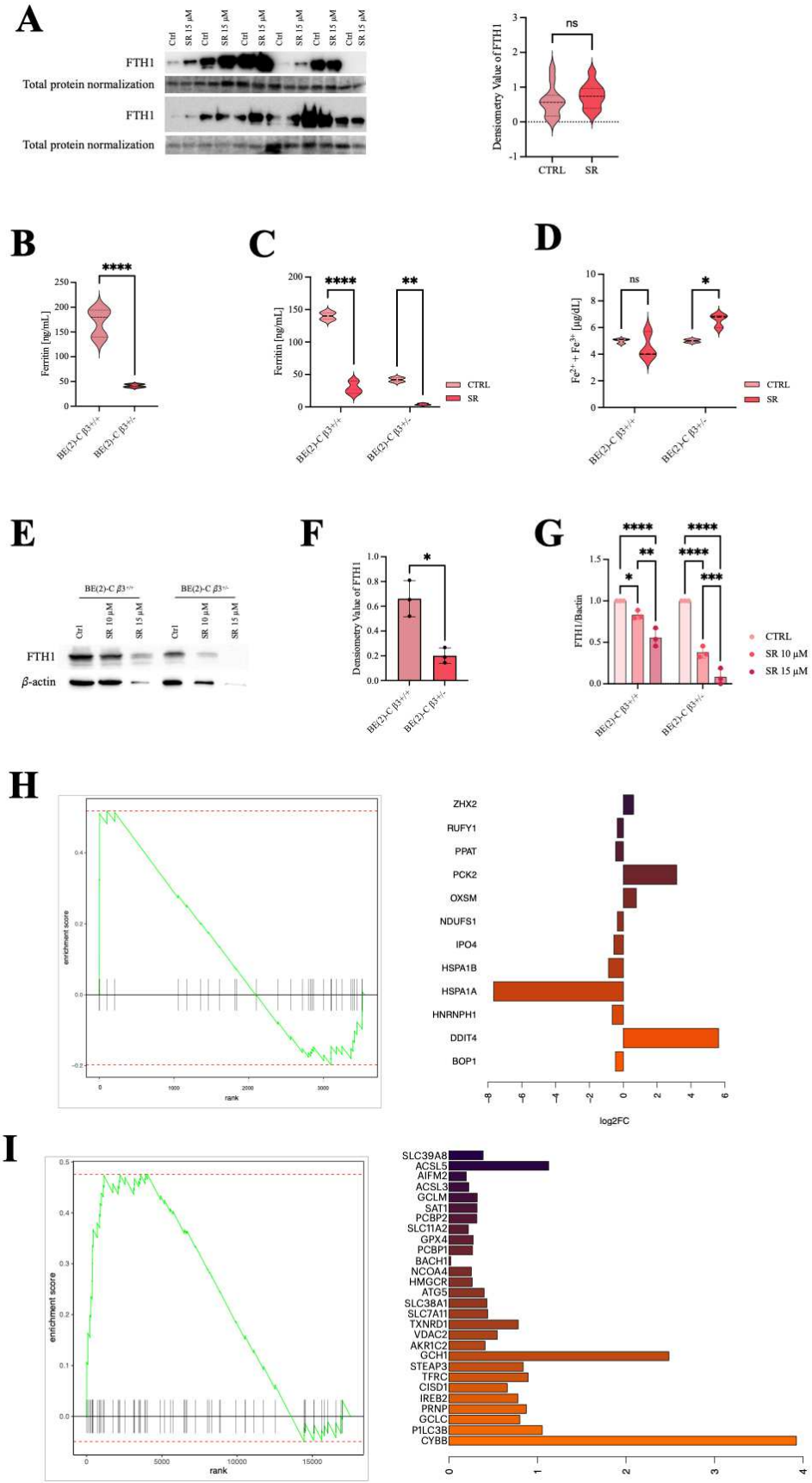
A
Ctrl
SR 15 µM
FTH1
Total protein normalization
FTH1
Total protein normalization
Densiometry Value of FTH1
ns
CTRL
SR
B
Ferritin [ng/mL]
****
BE(2)-C β3+/+
BE(2)-C β3+/-
C
Ferritin [ng/mL]
****
**
CTRL
SR
D
Fe2+ + Fe3+ [µg/dL]
ns
*
CTRL
SR
E
BE(2)-C β3+/+
BE(2)-C β3+/-
Ctrl
SR 10 µM
SR 15 µM
FTH1
β-actin
F
Densiometry Value of FTH1
*
G
FTH1/Bactin
CTRL
SR 10 µM
SR 15 µM
H
enrichment score
rank
ZHX2
RUFY1
PPAT
PCK2
OXSM
NDUFS1
IPO4
HSPA1B
HSPA1A
HNRNPH1
DDIT4
BOP1
log2FC
I
enrichment score
rank
SLC39A8
ACSL5
AIFM2
ACSL3
GCLM
SAT1
PCBP2
SLC11A2
GPX4
PCBP1
BACH1
NCOA4
HMGCR
ATG5
SLC38A1
SLC7A11
TXNRD1
VDAC2
AKR1C2
GCH1
STEAP3
TFRC
CISD1
IREB2
PRNP
GCLC
P1LC3B
CYBB

300

2.4. Cobas® 8000-based multiplexed screening uncovers metabolic signatures of ferroptosis across cancer models

Considering the extensive range of analytes accessible on the Cobas® 8000 platform and the proven reliability of its analytical performance through validation against orthogonal methods, we broadened our investigation to encompass additional cellular stress biomarkers beyond FTH1 and iron, specifically LDH and lactate. Both LDH and lactate are well-established indicators of metabolic dysfunction and cellular injury: high LDH levels reflected membrane damage and cytolysis, while altered lactate concentration revealed changes in glycolytic flux [54]. Although neither biomarker is exclusively specific for ferroptosis, these parameters commonly complement cell death processes and offer complementary information regarding the metabolic status of stressed cells. In our recent studies, we have shown that pharmacological inhibition of β3-AR with SR reduced glycolytic activity in cancer cells, with LDH and lactate representing measurable downstream readouts. Consistently, A673 ES cells treated with SR 15 μM for 24, 48, and 72 h exhibited a significant reduction in LDH release (*Fig. 5A*) with a concomitant increase in lactate concentrations (*Fig. 5B*), indicating both impaired glycolysis and drug-induced cytotoxicity. We further evaluated this response in leukemia models, applying SR either alone or in combination with deferoxamine (DFX) 0.1 μM, which acts as an iron chelator and prevents iron-dependent oxidative damage, thereby suppressing ferroptosis. As expected, SR alone led to a marked reduction in LDH, while co-treatment with DFX restored LDH release to basal levels (*Fig. 5C*), indicating that the observed effect was dependent on ferroptotic signaling. Lactate responses varied across leukemia subtypes: in CCRF-CEM cells, SR-induced lactate reduction was reversed by DFX, whereas Molt-3 cells showed no significant change, and Jurkat cells, consistent with their insensitivity to SR, persisted unaffected (*Fig. 5D*). In contrast, MV4;11 cells did not display significant alterations in either LDH (*Fig. 5E*) or lactate (*Fig. 5F*) under any treatment condition, suggesting that ADRB3 inhibition does not impact glycolytic metabolism in this model. For lactate and LDH assays, quality control performance was monitored using Levy–Jennings plots, as was done for iron and FTH1. These charts confirmed the strength and reproducibility of the measurements across all time points. Representative Levy–Jennings plots for all analytes are provided in the Supplementary Materials (*S1 d,e*). Moreover, to assess the impact of sample preservation on assay reproducibility, paired measurements were performed on fresh and frozen aliquots. For iron and lactate quantification, only minimal variation was detected between the two

conditions, confirming the high stability of these analytes. In contrast, FTH1 and LDH displayed a more pronounced difference between fresh and frozen samples; however, this shift was consistent across all replicates. This systematic deviation suggests that, once an appropriate correction factor is established, frozen samples can be reliably compared with fresh samples for both FTH1 and LDH measurements (*Supplementary Table S4*). Taken together, these results highlight the ability of the Cobas® 8000 to detect nuanced changes in metabolic and damage-associated biomarkers with high sensitivity and reproducibility. While further investigation is necessary to clarify the mechanistic links between ADRB3 signaling, glycolysis, and ferroptosis, our data underscore how Cobas® 8000-based assays can extend beyond classical ferroptosis markers, enabling rapid, multiplexed screening of diverse analytes. This versatility positions the platform as a powerful first-line tool for large-scale functional studies in cancer biology.

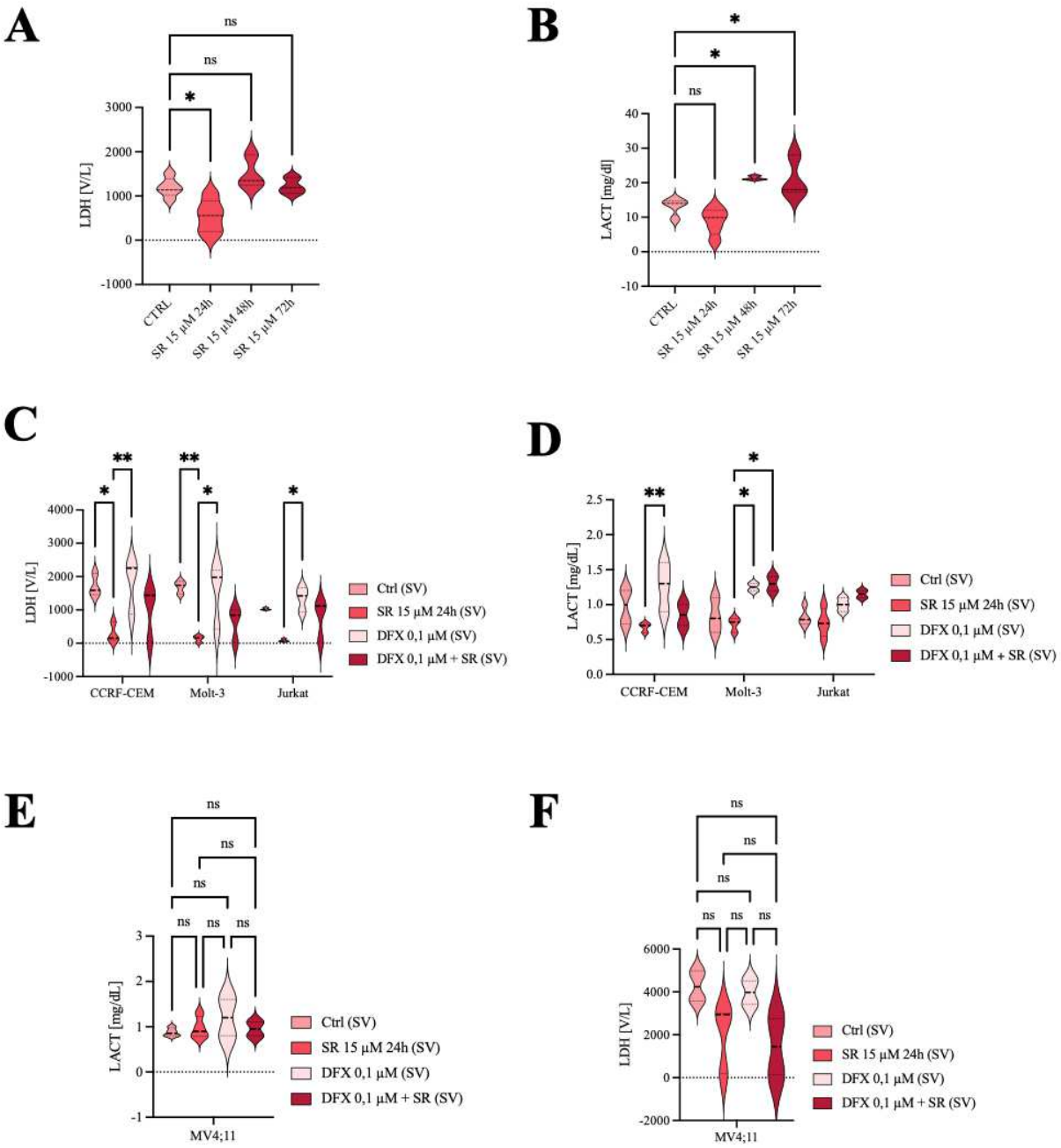

3. Discussion

Our study showed that the Cobas® 8000 platform, widely used in clinical diagnostics, can be repurposed to investigate ferroptosis in translational oncology. By adapting standardized assays for FTH1 and free iron, we established a consistent, fast, and operator-independent approach that faithfully reproduced results obtained with conventional techniques such as WB and RNA sequencing. The ability of Cobas® 8000 to discriminate ferroptosis-sensitive from resistant

pediatric cancer models highlights its potential as a versatile screening tool for drug discovery and repositioning.

A significant advantage of this methodology resides in its dual functionality at the interface between laboratory research and clinical practice. Unlike traditional assays that require extensive preparation, large sample volumes, and lengthy turnaround times, Cobas® 8000 enables the analysis of multiple analytes in a few minutes, through the same protocols, calibrations, and reference ranges already validated in clinical laboratories. In contrast, WB typically requires several days from protein extraction to quantification, involving multiple antibody-dependent steps that are susceptible to technical variability and operator-dependent bias [55,56]. Direct comparison underscores how Cobas® 8000 not only accelerates the workflow but also reduces experimental noise, thereby improving reproducibility and enabling scalable applications (*Fig. 6*).

This standardization creates a unique bridge between preclinical research and patient management: the same FTH1 or iron measurements performed on tumor cell lines can be seamlessly compared to values obtained from patient samples [57]. Such continuity paves the way for integrated translational pipelines, where findings from in vitro models can be rapidly contextualized in the clinical setting [58,59].

The versatility of the Cobas® 8000 system further broadens its applications. In addition to ferroptosis-related markers, we showed that other stress- and metabolism-associated parameters, such as LDH and lactate, can be measured with equal sensitivity and reproducibility. The combination of photometric and immunoassay modules, supported by electrochemiluminescence technology, enables multiplexed profiling of diverse analytes from the same sample. This capability expands the scope of high-throughput screening, providing both mechanistic insights and clinically actionable biomarkers. Importantly, the analytical spectrum of Cobas® 8000 assays also opens opportunities for systematic exploration of cellular metabolism. A wide range of clinically validated analytes can be readily quantified across multiple metabolic pathways, as exemplified in *Table S5.*

Nonetheless, some limitations must be acknowledged. While Cobas® 8000 provides precise quantification, it does not capture subcellular iron dynamics or the spatial heterogeneity of tumor tissues, which may require complementary imaging or single-cell technologies. Moreover, interpreting nonspecific markers such as LDH or lactate requires careful contextualization, since their modulation may reflect multiple cell death pathways. Finally, although our study validates

Cobas® 8000 in cellular models, further work is needed to assess its utility in large patient cohorts and to explore integration with multi-omic approaches.

Looking forward, the implementation of Cobas® 8000-based assays in drug discovery programs offers a concrete opportunity to accelerate therapeutic development. The possibility to screen large panels of compounds across multiple cell lines and primary cells—healthy or diseased—could streamline the identification of ferroptosis modulators and reduce translational gaps. In oncology, the longitudinal monitoring of prognostic analytes such as FTH1 in patients could inform both treatment stratification and therapeutic response. In this context, the growing clinical interest in ferroptosis-oriented therapeutic strategies highlights the need for simple and standardized tools to monitor ferroptosis-associated responses. Examples include the ongoing trial evaluating carbon nanoparticle-loaded iron [CNSI-Fe(II)] in advanced solid tumors, NCT06048367, and the trial investigating sulfasalazine in metastatic colorectal cancer, NCT06134388. Although comparable ferroptosis-oriented trials are not yet clearly established in pediatric oncology, preclinical evidence increasingly supports ferroptosis-related vulnerabilities in pediatric tumors, including neuroblastoma[1,2]. This gap further emphasizes the need for clinically compatible approaches capable of monitoring iron-related and metabolic biochemical responses. Cobas® 8000-based measurement of analytes such as free iron, FTH1, LDH, and lactate could therefore provide a rapid readout of ferroptosis-associated cellular states, helping to prioritize pediatric tumor models or patient-derived samples for deeper mechanistic validation.

Importantly, this technology is already available in many hospital laboratories worldwide, often in close collaboration with research institutions. Its immediate accessibility, combined with minimal adaptation requirements, positions Cobas® 8000 not only as a methodological innovation but also as a practical, ready-to-use bridge between bench and bedside. In this sense, the platform embodies a paradigm shift: transforming a routine clinical instrument into a powerful research tool that can shape the future of translational oncology.

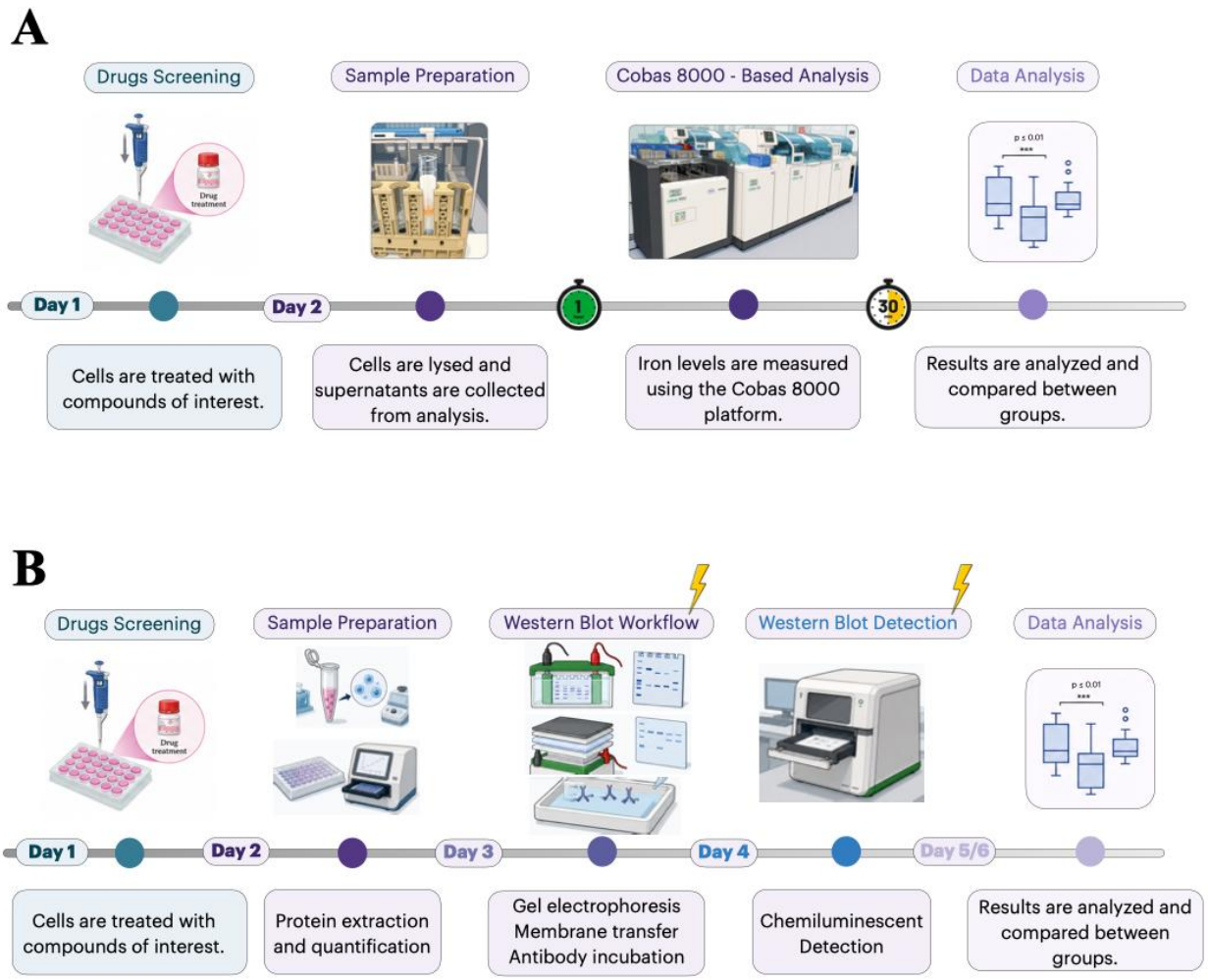

Declaration of Competing Interest

The authors declare no competing interests.

Acknowledgments

This work was supported by the Fondazione Umberto Veronesi through the Postdoctoral Fellowship 2025 awarded to Cristina Banella. We thank Fondazione Ospedale Pediatrico Meyer IRCCS, Florence, Italy. This work was also supported in part, by funds from the "Current Research Annual Funding of The Italian Ministry of Health.

Figure Legends

Figure 1. Analytical setup for FTH1 quantification using Cobas® 8000. Serial dilution of a ferritin human sample with known concentration (**A**) and of MV4;11 cellular protein lysates (**B**) in supplemented lysis buffer to assess matrix compatibility and assay linearity. (**C**) Schematic of the

Roche Cobas® 8000 sandwich immunoassay used to measure FTH1: ferritin antigen in the sample is captured by a biotinylated anti-ferritin antibody bound to streptavidin-coated microparticles and detected with a ruthenium-labeled anti-ferritin antibody and tripropylamine (TPA) co-reactant. A chemioluminescent (ECL) signal is generated during the voltage pulse cycle and proportional to FTH1 concentration (light accumulation). (**D**) Daily Levey–Jennings charts of FTH1, with values monitored against instrument-specific calibration and manufacturer's recommended ranges. (**E**) Dose–response curves of secreted FTH1 in pediatric tumor cell lines A673 (ES) and CCRF-CEM (LAL-T) after treatment with increasing concentrations of erastin 0-40 μM (x-axis, log scale). (**F**) Time course of FTH1 release. A673 and CCRF-CEM cells were treated with erastin 10 μM for 24,48, and 72h. FTH1 concentration (ng/mL) is plotted versus time (x-axis on log scale, in minutes). Each point represents mean ± SEM (N≥3) (C–D). Data were analyzed by nonlinear regression (curve fitting, least-squares method, Prism 10). Curves represent the best-fit model with R^2 = 0.9.

Figure 2. Workflow for iron measurement and kinetics of iron release in tumor cell lines. (**A**) Experimental workflow diagram. Cultured A673 or CCRF-CEM (LAL-T) cells were drug treated, then the supernatant was collected and analyzed with Cobas® 8000. After treatment, the culture medium was processed for ferrous/ferric iron content. The inset cartoon illustrates the chemical principle of the iron assay: Fe^3+ is released from TRF1 (acid dissociation), reduced to Fe^2+ by ascorbate, and then quantified via the ferrozine colorimetric reaction (magenta complex, absorbance proportional to Fe^2+). (**B**) Daily Levey–Jennings charts of FTH1, with values monitored against instrument-specific calibration and manufacturer's recommended ranges. (**C**) Time-dependent increase of iron in the medium for A673 and CCRF-CEM cell line after 24,48, and 72h treatment with erastin 10 μM. (**D**) Data were analyzed by nonlinear regression (curve fitting, least-squares method, Prism 10). Curves represent the best-fit model with R^2 = 0.044 and R^2 = 0.25 for A673 and CCRF-CEM, respectively. Each point represents mean ± SEM (N≥3).

Figure 3. Effects of the SR on FTH1 secretion and iron content in PBMCs and pediatric tumor cell line models. PBMCs from healthy donors and pediatric cancer cell lines were treated with SR 15 μM for 24 h, and FTH1 and free iron concentrations were measured on the Cobas® 8000 analyzer. **(A–B)** FTH1 (A) and iron (B) levels in PBMCs, shown together with corresponding estimation plots. No significant changes were detected. Changes in FTH1 concentration in AML (MV4;11)

(**C**), T-cell ALL (CCRF-CEM, Molt-3, Jurkat) (**D**), ES (A673) (**E**), and NB (Be2C) (**F**) cell lines. Significant reductions were observed in MV4;11, CCRF-CEM, Molt-3, A673, and Be2C, but not in Jurkat cells. **(E–F)** Changes in free iron levels in the same cell lines. Increased iron release was detected in MV4;11, Molt-3, and A673, but not in CCRF-CEM, Jurkat, or Be2C. The experiments were conducted in triplicate. Statistical significances were evaluated through Kruskal–Wallis one-way ANOVA and posterior Tukey's Multiple Comparison Test. Data are presented as mean ± SEM. The experiments were conducted in triplicate. Statistical significances were evaluated through Kruskal–Wallis one-way ANOVA and posterior Tukey's Multiple Comparison Test (* $p \leq 0.01$ ** $p \leq 0.001$; *** $p \leq 0.0001$; **** $p \leq 0.0001$).

Figure 4. Validation of Cobas® 8000 assay and role of ADRB3 in ferroptosis. (**A**) WB of FTH1 in PBMCs of healthy donors treated with SR 15 μM for 24h and relative densitometric quantification. (**B–D**) Cobas® 8000 quantification of basal FTH1, SR-induced ferritin reduction, and iron release in ADRB3$^{+/-}$ vs. WT Be2C cells. (**E–G**) WB and densitometry showing lower FTH1 expression and enhanced SR response in ADRB3$^{+/-}$ cells. Blots shown represent the best exposure times selected from multiple experiments, with dividing lines indicating where images have been cropped from different parts of the same gel or from different gels. Full-length blots with multiple exposure times are provided in the Supplementary Figure (**S1**). Data are presented as mean ± SEM. Two-way Anova assessed statistical significance, multiple comparisons followed by Tukey post-hoc test (* $p \leq 0.01$, ** $p \leq 0.001$; *** $p \leq 0.0001$; **** $p \leq 0.0001$). (**H–I**) RNA-seq and GSEA revealing ferroptosis pathway activation and upregulation of ferroptosis-related genes after SR in ES and BE(2)-C cells.

Figure 5. Cobas® 8000 measurements of LDH and lactate across cell lines and treatments. Cobas® 8000 quantification of LDH (**A**) and lactate (**B**) in A673 cells treated with SR 15 μM for 24, 48, and 72 h or vehicle control; violin plots show data distribution with pairwise comparisons at each time point. (**C–D**) Cobas-measured LDH (C) and lactate (**D**) levels CCRF-CEM, Molt-3, and Jurkat cells after 24 h treatment with SR 15 μM, DFX 0.1 μM, and combined DFX+SR conditions, showing treatment- and cell line–dependent responses. (**E–F**) Corresponding Cobas® 8000 assays for lactate (**E**) and LDH (**F**) in MV4;11 acute myeloid leukemia cells, demonstrating no significant treatment effects. Data are presented as mean ± SEM from three independent experiments. A two-way ANOVA was used to assess statistical significance, followed by Tukey's multiple comparisons test. Statistical annotations: ns, not significant; *P < 0.05; **P < 0.01; ****P < 0.0001.

Figure 6. Streamlined Cobas® 8000 pipeline versus traditional WB (**A**) Cobas® 8000 workflow: drug screening (day 1), sample preparation (day 2), automated Cobas® 8000 analysis (~60 min run + 30 min readout), and data analysis—a streamlined, instrument-centric pipeline compatible with high-throughput screening. (**B**) WB workflow: drug screening (day 1), protein lysis and quantification (day 2), gel electrophoresis and transfer (day 3), antibody incubations and chemiluminescent detection (days 4–6), followed by data analysis—a multi-day, manual protocol requiring sequential hands-on steps. Lightning-bolt icons indicate critical steps prone to technical variability: sample handling/normalization, membrane transfer, antibody incubations, and imaging procedures that increase experimental time, labor, and inter-assay variation. The comparison highlights the trade-off between throughput/reproducibility (Cobas® 8000) versus molecular specificity/validation (WB).

Declarations

Ethical Approval and Accordance

The study was conducted using established human cancer cell lines and peripheral blood mononuclear cells (PBMCs) isolated from healthy donors. The collection and use of human biological samples from healthy donors were conducted within the framework of the observational study BETA 3 2019, approved by the Regional Ethics Committee of Tuscany for Pediatric Studies (Comitato Etico Regionale della Toscana – Pediatrico; favorable opinion reference CET_14/2023, issued on July 27, 2023). All procedures involving human biological samples were performed in accordance with the Declaration of Helsinki and applicable institutional and national ethical guidelines and regulations.

Consent to Participate declaration

Written informed consent was obtained from all healthy adult donors or from the parents or legal guardians of pediatric donors, as applicable. Age-appropriate assent was obtained from pediatric donors in accordance with the approved study protocol.

Consent to Publish declaration

Not applicable. The manuscript does not contain identifiable individual participant data or images.

Clinical Trial Registration

Not applicable. This manuscript does not report the results of a clinical trial. The clinical trial

registration number NCT06048367 mentioned in the manuscript refers to an external clinical trial cited solely for background information and is not associated with the present study.

Data availability

Data will be made available on request to the corresponding author.

Author Contributions

C.B., M.A., and M.C. conceived the study and designed the research. C.B., M.A., L.B., R.A., L.M., and B.P. established and optimized the experimental methodology. C.B., M.A., L.B., M.V., and M.C. performed the experiments and data acquisition. C.B. and M.C. prepared the figures and visualizations. A.T., F.B., and M.C. supervised the project and provided conceptual guidance. C.B., M.A., and M.C. wrote the original draft, and C.B., M.A., A.P., F.P., P.S., S.T, and M.C. reviewed and edited the final manuscript. All authors read and approved the submitted version.

Supplemental Information

All data needed to evaluate the conclusions in the paper are present in the main text and/or the Supplementary Materials.

References

[1] H. Deng, J. Tang, Y. Xu, L. Wu, J. Zhang, H. Chen, Z. Wang, R. Yang, W. Gao, Z. He, Mitochondrial Damage-induced Ferroptosis: The Molecular Mechanism by Which Psoralen Inhibits the Proliferation and Invasion of Non-small-cell Lung Cancer Cells, In Vivo 39 (2025) 2681–2702. https://doi.org/10.21873/invivo.14068.

[2] C. Yang, S. Li, L. Wang, Engineered iron oxide nanoplatforms: reprogramming immunosuppressive niches for precision cancer theranostics, Mol Cancer 24 (2025) 225. https://doi.org/10.1186/s12943-025-02443-2.

[3] L. Zhao, Z. Xu, L. Ren, S. Zheng, J. Gao, H. Che, A. Zhang, Investigating the relationship between peripheral blood transferrin receptor protein and tumor cell ferroptosis, invasion, and metastasis in bladder cancer, Sci Rep 15 (2025) 32197. https://doi.org/10.1038/s41598-025-12187-0.

[4] J.-C. Shir, P.-Y. Chen, C.-H. Kuo, C.-H. Hsieh, H.-Y. Chang, H.-C. Lee, C.-H. Huang, C.-H. Hsu, W.-M. Hsu, H.-C. Huang, H.-F. Juan, DHODH Blockade Induces Ferroptosis in Neuroblastoma by Modulating the Mevalonate Pathway, Mol Cell Proteomics 24 (2025) 101014. https://doi.org/10.1016/j.mcpro.2025.101014.

[5] H. Alborzinia, A.F. Flórez, S. Kreth, L.M. Brückner, U. Yildiz, M. Gartlgruber, D.I. Odoni, G. Poschet, K. Garbowicz, C. Shao, C. Klein, J. Meier, P. Zeisberger, M. Nadler-Holly, M. Ziehm, F. Paul, J. Burhenne, E. Bell, M. Shaikhkarami, R. Würth, S.A. Stainczyk, E.M. Wecht, J. Kreth, M. Büttner, N. Ishaque, M. Schlesner, B. Nicke, C. Stresemann, M. Llamazares-Prada, J.H. Reiling, M. Fischer, I. Amit, M. Selbach, C. Herrmann, S. Wölfl, K.-O. Henrich, T. Höfer, A. Trumpp, F. Westermann, MYCN mediates cysteine addiction and sensitizes neuroblastoma to ferroptosis, Nat Cancer 3 (2022) 471–485. https://doi.org/10.1038/s43018-022-00355-4.

[6] H. Chen, J. Hu, X. Xiong, H. Chen, B. Lin, Y. Chen, Y. Li, D. Cheng, Z. Li, AURKA inhibition induces Ewing's sarcoma apoptosis and ferroptosis through NPM1/YAP1 axis, Cell Death Dis 15 (2024) 99. https://doi.org/10.1038/s41419-024-06485-0.

[7] Y. Tao, L. Wei, H. You, Ferroptosis-related gene signature predicts the clinical outcome in pediatric acute myeloid leukemia patients and refines the 2017 ELN classification system, Front Mol Biosci 9 (2022) 954524. https://doi.org/10.3389/fmolb.2022.954524.

[8] A. Catapano, F. Cimmino, L. Petrella, A. Pizzella, M. D'Angelo, K. Ambrosio, F. Marino, A. Sabbatini, M. Petrelli, B. Paolini, L. Lucchin, G. Cavaliere, L. Cristino, M. Crispino, G. Trinchese, M.P. Mollica, Iron metabolism and ferroptosis in health and diseases: The crucial role of mitochondria in metabolically active tissues, J Nutr Biochem 140 (2025) 109888. https://doi.org/10.1016/j.jnutbio.2025.109888.

[9] J. Chifman, R. Laubenbacher, S.V. Torti, A systems biology approach to iron metabolism, Adv Exp Med Biol 844 (2014) 201–225. https://doi.org/10.1007/978-1-4939-2095-2_10.

[10] C. Berndt, C.H. Lillig, Glutathione, Glutaredoxins, and Iron, Antioxid Redox Signal 27 (2017) 1235–1251. https://doi.org/10.1089/ars.2017.7132.

[11] F.W. Outten, E.C. Theil, Iron-based redox switches in biology, Antioxid Redox Signal 11 (2009) 1029–1046. https://doi.org/10.1089/ars.2008.2296.

[12] A.M. Battaglia, R. Chirillo, I. Aversa, A. Sacco, F. Costanzo, F. Biamonte, Ferroptosis and Cancer: Mitochondria Meet the "Iron Maiden" Cell Death, Cells 9 (2020) 1505. https://doi.org/10.3390/cells9061505.

[13] D. Liang, A.M. Minikes, X. Jiang, Ferroptosis at the intersection of lipid metabolism and cellular signaling, Mol Cell 82 (2022) 2215–2227. https://doi.org/10.1016/j.molcel.2022.03.022.
[14] S.J. Dixon, K.M. Lemberg, M.R. Lamprecht, R. Skouta, E.M. Zaitsev, C.E. Gleason, D.N. Patel, A.J. Bauer, A.M. Cantley, W.S. Yang, B. Morrison, B.R. Stockwell, Ferroptosis: an iron-dependent form of nonapoptotic cell death, Cell 149 (2012) 1060–1072. https://doi.org/10.1016/j.cell.2012.03.042.
[15] X. Liu, E.C. Theil, Ferritin as an iron concentrator and chelator target, Ann N Y Acad Sci 1054 (2005) 136–140. https://doi.org/10.1196/annals.1345.016.
[16] P. Armand, H.T. Kim, C.S. Cutler, V.T. Ho, J. Koreth, E.P. Alyea, R.J. Soiffer, J.H. Antin, Prognostic impact of elevated pretransplantation serum ferritin in patients undergoing myeloablative stem cell transplantation, Blood 109 (2007) 4586–4588. https://doi.org/10.1182/blood-2006-10-054924.
[17] W.P. Faulk, B.-L. Hsi, P.J. Stevens, TRANSFERRIN AND TRANSFERRIN RECEPTORS IN CARCINOMA OF THE BREAST, The Lancet 316 (1980) 390–392. https://doi.org/10.1016/S0140-6736(80)90440-7.
[18] W. Wang, M.A. Knovich, L.G. Coffman, F.M. Torti, S.V. Torti, Serum ferritin: Past, present and future, Biochim Biophys Acta 1800 (2010) 760–769. https://doi.org/10.1016/j.bbagen.2010.03.011.
[19] B.S. Skikne, C.H. Flowers, J.D. Cook, Serum transferrin receptor: a quantitative measure of tissue iron deficiency, Blood 75 (1990) 1870–1876.
[20] J. Riemer, H.H. Hoepken, H. Czerwinska, S.R. Robinson, R. Dringen, Colorimetric ferrozine-based assay for the quantitation of iron in cultured cells, Analytical Biochemistry 331 (2004) 370–375. https://doi.org/10.1016/j.ab.2004.03.049.
[21] M. Tenopoulou, T. Kurz, P.-T. Doulias, D. Galaris, U.T. Brunk, Does the calcein-AM method assay the total cellular “labile iron pool” or only a fraction of it?, Biochem J 403 (2007) 261–266. https://doi.org/10.1042/BJ20061840.
[22] V. Pandey, A.K. Mayank, J.A. Wohlschlegel, Analyzing Iron and Oxygen-Regulated Protein Complex Formation Using Proteomic Mass Spectrometry, Methods Mol Biol 2648 (2023) 155–166. https://doi.org/10.1007/978-1-0716-3080-8_10.
[23] J.C. Crack, N.E. Le Brun, Native Mass Spectrometry of Iron-Sulfur Proteins, Methods Mol Biol 2353 (2021) 231–258. https://doi.org/10.1007/978-1-0716-1605-5_13.
[24] C.T.N. Nguyen, S.M. Kim, Y.P. Kang, Mass spectrometry-based approaches to explore metabolism regulating ferroptosis, BMB Rep 55 (2022) 413–416. https://doi.org/10.5483/BMBRep.2022.55.9.109.
[25] J. Yamazaki, I. Inoue, A. Arakawa, S. Karakawa, K. Takahashi, A. Nakayama, Simultaneous quantification of oligo-nucleic acids and a ferritin nanocage by size-exclusion chromatography hyphenated to inductively coupled plasma mass spectrometry for developing drug delivery systems, Anal Methods 14 (2022) 2219–2226. https://doi.org/10.1039/d2ay00068g.
[26] T. Mahmood, P.-C. Yang, Western blot: technique, theory, and trouble shooting, N Am J Med Sci 4 (2012) 429–434. https://doi.org/10.4103/1947-2714.100998.
[27] B.N. Loke, M.K. Wong, K.D. Tawng, C.H. Kuick, S. Jain, D. Lian, E. Wagner, Y. Zou, V. Ganesan, S.W. Sim, Y.T. Lee, F. Chin, M.Y. Chan, A.M. Tan, B.T. Teh, S.Y. Soh, K.T.E. Chang, A.H.P. Loh, Clinical, pathological and loss of heterozygosity differences in Wilms tumors between Asian and non-Asian children, Int J Cancer 144 (2019) 1234–1242. https://doi.org/10.1002/ijc.31946.

[28] X. Pan, X. Pei, H. Huang, N. Su, Z. Wu, Z. Wu, X. Qi, One-in-one individual package and delivery of CRISPR/Cas9 ribonucleoprotein using apoferritin, J Control Release 337 (2021) 686–697. https://doi.org/10.1016/j.jconrel.2021.08.015.
[29] E. Katsman, S. Orlanski, F. Martignano, I. Fox-Fisher, R. Shemer, Y. Dor, A. Zick, A. Eden, I. Petrini, S.G. Conticello, B.P. Berman, Detecting cell-of-origin and cancer-specific methylation features of cell-free DNA from Nanopore sequencing, Genome Biol 23 (2022) 158. https://doi.org/10.1186/s13059-022-02710-1.
[30] K. O'Neill, E. Pleasance, J. Fan, V. Akbari, G. Chang, K. Dixon, V. Csizmok, S. MacLennan, V. Porter, A. Galbraith, C.J. Grisdale, L. Culibrk, J.H. Dupuis, R. Corbett, J. Hopkins, R. Bowlby, P. Pandoh, D.E. Smailus, D. Cheng, T. Wong, C. Frey, Y. Shen, E. Lewis, L.F. Paulin, F.J. Sedlazeck, J.M.T. Nelson, E. Chuah, K.L. Mungall, R.A. Moore, R. Coope, A.J. Mungall, M.K. McConechy, L.M. Williamson, K.A. Schrader, S. Yip, M.A. Marra, J. Laskin, S.J.M. Jones, Long-read sequencing of an advanced cancer cohort resolves rearrangements, unravels haplotypes, and reveals methylation landscapes, Cell Genom 4 (2024) 100674. https://doi.org/10.1016/j.xgen.2024.100674.
[31] M. Hedayati, S.A. Razavi, S. Boroomand, S. Kheradmand Kia, The impact of pre-analytical variations on biochemical analytes stability: A systematic review, J Clin Lab Anal 34 (2020) e23551. https://doi.org/10.1002/jcla.23551.
[32] R.A. Abraham, P.K. Agrawal, R. Acharya, A. Sarna, S. Ramesh, R. Johnston, A. de Wagt, N. Khan, A. Porwal, S.B. Kurundkar, A. Pandey, R. Pullakhandam, K.M. Nair, G.T. Kumar, H.P.S. Sachdev, U. Kapil, R. Saxena, S. Deb, A. Khera, L. Ramakrishnan, Effect of temperature and time delay in centrifugation on stability of select biomarkers of nutrition and non-communicable diseases in blood samples, Biochem Med (Zagreb) 29 (2019) 020708. https://doi.org/10.11613/BM.2019.020708.
[33] J.-L. Sun, N.-P. Zhang, R.-C. Xu, G.-C. Zhang, Z.-Y. Liu, W. Abuduwaili, F. Wang, X.-N. Yu, X. Shi, G.-Q. Song, H. Wu, T.-T. Liu, X.-Z. Shen, B. Deng, S.-Q. Weng, L. Dong, J.-M. Zhu, Tumor cell-imposed iron restriction drives immunosuppressive polarization of tumor-associated macrophages, J Transl Med 19 (2021) 347. https://doi.org/10.1186/s12967-021-03034-7.
[34] A. Sacco, A.M. Battaglia, C. Botta, I. Aversa, S. Mancuso, F. Costanzo, F. Biamonte, Iron Metabolism in the Tumor Microenvironment-Implications for Anti-Cancer Immune Response, Cells 10 (2021) 303. https://doi.org/10.3390/cells10020303.
[35] C. Pfeifhofer-Obermair, P. Tymoszuk, V. Petzer, G. Weiss, M. Nairz, Iron in the Tumor Microenvironment-Connecting the Dots, Front Oncol 8 (2018) 549. https://doi.org/10.3389/fonc.2018.00549.
[36] L. Hou, J. Lu, X. Jiang, X. Guo, C. Ma, X. Cheng, Analytical evaluation of three soluble transferrin receptor measurement systems for diagnosis of iron deficiency anemia: A retrospective study, J Clin Lab Anal 34 (2020) e23342. https://doi.org/10.1002/jcla.23342.
[37] S. Kolbe-Busch, J. Lotz, G. Hafner, N.J.C. Blanckaert, G. Claeys, G. Togni, J. Carlsen, R. Röddiger, L. Thomas, Multicenter evaluation of a fully mechanized soluble transferrin receptor assay on the Hitachi and cobas integra analyzers. the determination of reference ranges, Clin Chem Lab Med 40 (2002) 529–536. https://doi.org/10.1515/CCLM.2002.091.
[38] M.K. Bohn, V. Higgins, S. Asgari, F. Leung, B. Hoffman, J. Macri, K. Adeli, Paediatric reference intervals for 17 Roche cobas 8000 e602 immunoassays in the CALIPER cohort of healthy children and adolescents, Clin Chem Lab Med 57 (2019) 1968–1979. https://doi.org/10.1515/cclm-2019-0707.

[39] S. Lim, K. Lee, H.-Y. Woo, H. Park, M.-J. Kwon, Evaluation of Cobas 8000 Analyzer Series Module e801 Analytical Performance, Ann Clin Lab Sci 49 (2019) 372–379.
[40] B. Wan, R. Augustin, M.K. Chan, J. Leblond, Z. Verjee, K. Adeli, Analytical performance and workflow evaluation of the Roche E170 modular immunoassay analyzer in a pediatric setting, Clin Biochem 38 (2005) 262–271. https://doi.org/10.1016/j.clinbiochem.2004.11.010.
[41] L. Gruber, A. Hausch, T. Mueller, Internal Quality Controls in the Medical Laboratory: A Narrative Review of the Basic Principles of an Appropriate Quality Control Plan, Diagnostics (Basel) 14 (2024) 2223. https://doi.org/10.3390/diagnostics14192223.
[42] Y. Zhang, H. Tan, J.D. Daniels, F. Zandkarimi, H. Liu, L.M. Brown, K. Uchida, O.A. O'Connor, B.R. Stockwell, Imidazole Ketone Erastin Induces Ferroptosis and Slows Tumor Growth in a Mouse Lymphoma Model, Cell Chem Biol 26 (2019) 623-633.e9. https://doi.org/10.1016/j.chembiol.2019.01.008.
[43] L. Wang, Y. Liu, T. Du, H. Yang, L. Lei, M. Guo, H.-F. Ding, J. Zhang, H. Wang, X. Chen, C. Yan, ATF3 promotes erastin-induced ferroptosis by suppressing system Xc, Cell Death Differ 27 (2020) 662–675. https://doi.org/10.1038/s41418-019-0380-z.
[44] X. Chen, R. Kang, G. Kroemer, D. Tang, Broadening horizons: the role of ferroptosis in cancer, Nat Rev Clin Oncol 18 (2021) 280–296. https://doi.org/10.1038/s41571-020-00462-0.
[45] B.R. Stockwell, Ferroptosis turns 10: Emerging mechanisms, physiological functions, and therapeutic applications, Cell 185 (2022) 2401–2421. https://doi.org/10.1016/j.cell.2022.06.003.
[46] T.A. Walmsley, P.M. George, R.T. Fowler, Colorimetric measurement of iron in plasma samples anticoagulated with EDTA, J Clin Pathol 45 (1992) 151–154. https://doi.org/10.1136/jcp.45.2.151.
[47] B. Löhr, V. El-Samalouti, W. Junge, H. Maatouk, A. Halabi, A. Fahle, S. Bossert-Reuther, M. Jung, C. Berding, I. Domke, Reference range study for various parameters on Roche clinical chemistry analyzers, Clin Lab 55 (2009) 465–471.
[48] M. Calvani, A. Dabraio, G. Bruno, V. De Gregorio, M. Coronnello, C. Bogani, S. Ciullini, G. la Marca, M. Vignoli, P. Chiarugi, M. Nardi, A.M. Vannucchi, L. Filippi, C. Favre, β3-Adrenoreceptor Blockade Reduces Hypoxic Myeloid Leukemic Cells Survival and Chemoresistance, Int J Mol Sci 21 (2020) 4210. https://doi.org/10.3390/ijms21124210.
[49] N. Nastasi, G. Bruno, C. Favre, M. Calvani, Role of β3-Adrenergic Receptor in Bone Marrow Transplant as Therapeutical Support in Cancer, Front Oncol 12 (2022) 889634. https://doi.org/10.3389/fonc.2022.889634.
[50] M. Calvani, A. Subbiani, M. Vignoli, C. Favre, Spotlight on ROS and β3-Adrenoreceptors Fighting in Cancer Cells, Oxid Med Cell Longev 2019 (2019) 6346529. https://doi.org/10.1155/2019/6346529.
[51] A. Pasha, A. Tondo, C. Favre, M. Calvani, Inside the Biology of the β3-Adrenoceptor, Biomolecules 14 (2024) 159. https://doi.org/10.3390/biom14020159.
[52] V.D. Ramseyer, J.G. Granneman, Adrenergic regulation of cellular plasticity in brown, beige/brite and white adipose tissues, Adipocyte 5 (2016) 119–129. https://doi.org/10.1080/21623945.2016.1145846.
[53] C. Cero, H.J. Lea, K.Y. Zhu, F. Shamsi, Y.-H. Tseng, A.M. Cypess, β3-Adrenergic receptors regulate human brown/beige adipocyte lipolysis and thermogenesis, JCI Insight 6 (2021) e139160. https://doi.org/10.1172/jci.insight.139160.

[54] P. Kumar, A. Nagarajan, P.D. Uchil, Analysis of Cell Viability by the Lactate Dehydrogenase Assay, Cold Spring Harb Protoc 2018 (2018). https://doi.org/10.1101/pdb.prot095497.
[55] J.J. Bass, D.J. Wilkinson, D. Rankin, B.E. Phillips, N.J. Szewczyk, K. Smith, P.J. Atherton, An overview of technical considerations for Western blotting applications to physiological research, Scand J Med Sci Sports 27 (2017) 4–25. https://doi.org/10.1111/sms.12702.
[56] T.A.J. Butler, J.W. Paul, E.-C. Chan, R. Smith, J.M. Tolosa, Misleading Westerns: Common Quantification Mistakes in Western Blot Densitometry and Proposed Corrective Measures, Biomed Res Int 2019 (2019) 5214821. https://doi.org/10.1155/2019/5214821.
[57] Q. Ru, Y. Li, L. Chen, Y. Wu, J. Min, F. Wang, Iron homeostasis and ferroptosis in human diseases: mechanisms and therapeutic prospects, Signal Transduct Target Ther 9 (2024) 271. https://doi.org/10.1038/s41392-024-01969-z.
[58] J. Cheng, Y. Song, Serum ferritin as a prognostic biomarker in CAR-T therapy for multiple myeloma: A meta-analysis, Biomol Biomed 25 (2025) 2416–2427. https://doi.org/10.17305/bb.2025.12129.
[59] K. Szymulewska-Konopko, J. Reszeć-Giełażyn, M. Małeczek, Ferritin as an Effective Prognostic Factor and Potential Cancer Biomarker, Curr Issues Mol Biol 47 (2025) 60. https://doi.org/10.3390/cimb47010060.

Supplementary Files

This is a list of supplementary files associated with this preprint. Click to download.

- SupplementaryM051126.docx